Trans. Phenom. Nano Micro Scales, 8(2): 126-136, Summer and Autumn 2020
DOI: 10.22111/tpnms.2020.28259.1167

ORIGINAL RESEARCH PAPER

# Analytical solution of a fully developed isothermal non-ideal gaseous slip flow in microchannels

***Mahdi Motamedian, Ahmad Reza Rahmati****

*Department of Mechanical Engineering, University of Kashan, Kashan, Iran*

*Received 2 January 2019; revised 23 October 2020; accepted 23 October 2020; available online 10 November 2020*

**ABSTRACT:** In this paper, the fully developed non-ideal gaseous slip flow in circular, parallel plates, and rectangular microchannels is analyzed analytically by using Navier-Stokes equations to obtain the analytical exact solution. Van der Waals equation is used as the state equation of non-ideal gas. It is assumed that the flow is isothermal, incompressible, steady state, two-dimensional and fully developed, slip flow regime with consideration the first and second orders boundary conditions. It is developed the models for predicting the local and mean velocity, normalized Poiseuille number, and the ratio of density for the first and second orders boundary conditions. The results show that the rarefication process and Poiseuille number are a function of the Knudsen number and the cross-section geometry and Poiseuille number is independent of fluid material properties, velocity, and temperature. Also, for circular microchannel, the rarefication process occurs faster than the others.

**KEYWORDS:** *Analytical solution; Microchannel; Non-ideal gaseous slip.*

## INTRODUCTION

Microchannels are the important part of microfluidic systems. The applications of microchannels are known as Micro-Electro-Mechanical Systems(MEMS),devices which have a characteristic length of less than 1mm and greater than1μm, microelectronic cooling, digital micro comp-ressors, micro-reactors, high-frequency fluid control systems, fuel cell technology, biochemical reaction chambers, infrared detectors, diode lasers and medical equipment. During past decades, various studies of fluid flow have been conducted in the microchannels

Arkilic et al.[1]analytically and experimentally studied ideal gas flow in a two-dimensional long microchannel .The effects of compressibility and rarefication phenomenon were investigated.

An analysis of rarefied gas flows in rectangular and annular ducts has been performed by applying analytical method by Ebert and Sparrow [2].The results showed that the effects of slip decrease velocity distribution and pressure drop is increased by the effect of compressibility.The rarefaction effects on the pressure drop for in compressible flow in a silicon rectangular,trapezoidal or double-trapezoidal cross section are evaluated by Morini et al.[3]. The effects of the Knudsen number and the cross-section aspect ratio in the friction factor reduction were discussed. Wimmer et al.[4] employed Laplace transform method to examine gas flow in two parallel plates. They used the Oseen equation to study the flow and compared the results with numerical method. Muzychka et al.[5-6] investigated a slip-flow through the non-circular and elliptic microchannels. The results indicate that accuracy of the developed model is 10% and 3% for elliptic and non-circular microchannels respectively.

Das and Tahmouresi [7] similuted an ideal fully developed gasous flow in elliptic microchannel by using integral transform technique. They investigated the effect of duct shape. The outputs show that normalized Poiseuille, friction factor and Reynolds number are good agreements with the previous results of rectangular and elliptic microchannels. Duan and Yovanovich [8] presented a simple model to predict the fiction factor and Reynolds number product f.Re for slip flow in different cross-section microchannels. The results shows that accuracy of Poiseuille number is 4.2% for all common duct shapes. Tahmouresi and Das [9] presented the fully developed gaseous slip-flow in symmetric and asymmetric parabolic micro-channels by applying the method of separation of variables. Normalized Poiseuille number, mass flow rate, and pressure distribution are compared with previous results. For small aspect ratio, it is found that results are good agreement with rectangular micro-channels. Wang and Li [10]developed Monte Carlo method based on the Enskog for simulating dense gas flow in the microchannel. The results demonstrate that high-density gas has important effects on the flow behavior and heat transfer properties. The high density leads to a lower coefficient of friction than ideal gases. Shi and Zhao[11] introduced the Enskog equation based lattice Boltzmann BGK model for simulating dense gas flow in the microchannel.

✉ *Corresponding Author Email: *ar_rahmati@kashanu.ac.ir*
Tel.: +989132073487; Note. This manuscript was submitted on January 2, 2019; approved on October 23, 2020; published online November 10, 2020.

**Nomenclature**

| | | | |
|---|---|---|---|
| $u$ | Gaseous velocity component (m/s) | $\overline{u_z^*}$ | Dimenstionless mean velocity |
| $f$ | Function | $u_z^*$ | Dimenstionless velocity |
| $V$ | Velocity vector (m/s) | $u_{z_0}$ | Velocity of microchannel center(m/s) |
| $r, \theta$ | Polar coordinates (m) | $\overline{u_z}$ | Mean velocity |
| $z$ | Coordinate in flow direction (m) | $r^*$ | Dimenstionless radius of circular microchannel |
| $x, y$ | Cartesian coordinates (m) | $\dot{m}$ | Mass flow rate (Kg/s) |
| $p$ | Pressure ($N/m^2$) | $y^*$ | Dimenstionless width of microchannel |
| $C_1$ | Constant coefficient (1/s) | $Po$ | Poiseuille number |
| $C_2$ | Constant coefficient (m/s) | $\upsilon_c$ | Critical Specific Volume |
| $A_2$ | Coefficient of the main models of second – order boundary condition | | **Greek symbol**s |
| $D_h$ | Hydraulic diameter (m) | $\rho$ | Gas density ($Kg/m^3$) |
| $P$ | Cross – sectional wetted perimeter (m) | $\mu$ | Viscosity($N.s/m^2$) |
| $r_2$ | Radius of circular microchannel radius (m) | $\sigma$ | Tangential momentum accomondation coefficient |
| $Kn$ | Knudsen number($\lambda/D_h$) | $\lambda$ | Molecular mean free path(m) |
| $A$ | Cross – sectional area ($m^2$) | | **Subscripts** |
| $h$ | Parallel plate microchannel cross- sectional width (m) | $r$ | r direction |
| $m$ | Parallel plate microchannel cross- sectional length (m) | $\theta$ | θ direction |
| $R$ | Specific gas constant ( J/Kg.°K ) | $z$ | z direction |
| $T$ | Temperature (°K) | $i$ | inlet |

Their results depict that clear slip is on the solid wall when the Knudsen number is of the order of $10^{-2}$. The magnitude of such a slip depends on the longitudinal aspect of the σ/δ gas.

He et al. [12] reported a discrete model based on the Boltzmann equation with a body force and a single relation time collision model for the simulation of non-ideal gas flow. Ihle and Kroll [13] simulated a non-ideal gas flow in a microchannel by means of thermal Lattice – Boltzmann method with potential energy. In this method, several distribution functions were proposed to apply the non-ideal gas and potential energy effects.

Hoseinalipour et al.[14]examined gas mixing in a T-shaped microchannel using the DSMC method.

Their results demonstrate an increase of the Knudsen number leads to reduce the coefficient of mixing. When the inlet pressure increases, the mixing length enhances. Hong et al.[15] studied a turbulent gas flow and heat transfer in a two-dimensional circular microchannel with constant thermal flux.

Their results show that the fanning friction factor is equal to the values given by the Blasius equation, and also the values of the Darcy friction factor are greater than the fanning friction factor.

Also, in another study, Huang et al.[16] repeated the previous study for laminar gas flow.

In outlet Mach numbers greater than 0.3, the total temperature is greater than the gas temperature for an incompressible flow due to the thermal energy converts to kinetic energy in the near the circular microchannel outlet.

Kawashima and Asako [17] carried out a nitrogen gas flow through a circular microchannel to investigate the friction factor and pressure drop.

Their results show that the quasi-local friction factor in the turbulent flow is only a function of the Re number and is about 12% to 20% higher than that of the Blasius. Rovenskaya [18] numerically studied compressible gas flow through three-dimensional microchannel with 90 degrees bend.

They used Navier–Stokes equations coupled with the first-order slip and Smoluchowski temperature jump boundary conditions. The results show that the inclusion of the bend in a microchannel increase mass flow rate and the pressure in bend is independent on an aspect ratio and similar to the two-dimensional microchannels.

The velocity profile is similar along the width and depth for an aspect ratio of more than four near centerline. Li and Hrnjak[19] investigated the effect of channel's diameter and length of the flow through microchannel evaporators, experimentally and numerically. It was found that the larger channel diameter and longer channel reveal less flow reversal with a lower frequency. In another study, they analyzed the effect of refrigerant specific volume differences and heat of vaporization on flow in microchannel evaporators.

Their results show that fluids with lower heat of vaporization and higher specific volume difference between vapor and liquid phase produce more reversed vapor flow [20].

Monsivais et al.[21] asymptotically and numerically studied the transpiration effect in the conjugate thermal creep flow between a rarefied gas flow and the lower wall of a thin microchannel.

It has been found when the temperature of the lower wall varies, the conjugate thermal creep phenomenon is produced.

Ghazanfari et al.[22] solved analytically the steady-state heat transfer equation in irregular domains under the homogenous and non-homogeneous boundary conditions. They used the conformal mapping method to obtain the exact solution.

Yang et al.[23] studied analytically the electroosmotic flow with pressure-driven in rectangular microchannels. The analyses show that the potential distribution of microflow is plug-like, and the velocity distribution of mixed flow is compound of the plug-like and paraboloid.

Few studies have been carried out in the analytical solution of gaseous slip flow in micro-channel and are mainly limited to ideal gas flow.

Todays, microchannels are fabricated with various cross-sectional geometry. Therefore, it is important to represent an analytical solution of non-ideal gaseous slip flow for microchannels to investigate the physical behavior of gases. For the specific problem presented in this paper, there has been no analytical solution for the non-ideal gaseous slip flow in microchannel based on differential formulation so far.

In this paper, a fully developed non-ideal gas flow through circular , parallel plate and rectangular microchannels with the first and second orders slip boundary conditions is analytically analyzed.

This study is carried out using the Navier- Stokes equations and the effects of wall slippage in different Knudsen numbers have been investigated.

Firstly, the general problem will be introduced to demonstrate the governing equations, the geometry of fluid flow and boundary condition equations. Secondly, the method will be applied in the circular, parallel plate and rectangular microchannels and the results will be validated by the exact solution. Finally, the results will be discussed.

## ANALYTICAL SOLUTION

A non-ideal gaseous slip flow is considered in a circular microchannel, a parallel plates microchannel and a rectangular microchannel (figures 1(a-c)).

In this study, it is assumed that the fully developed, steady-state, laminar, incompressible and constant fluid physical properties.

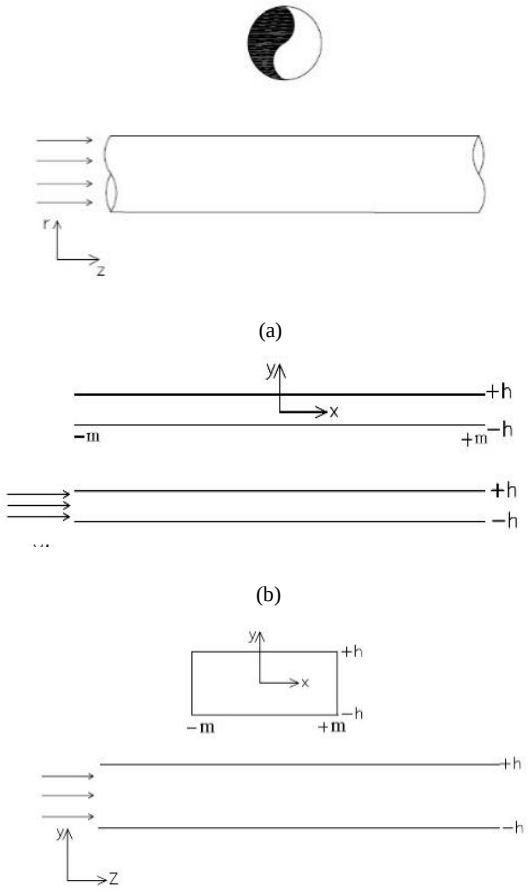



**Fig .1.** a) circular microchannel, b) parallel plate microchannel, c) rectangular microchannel

## Circular Microchannel

According to Figure 1a, the momentum equation for circular microchannel is:

$$\frac{1}{r}\frac{d}{dr}\left(r\frac{du_z}{dr}\right)=\frac{1}{\mu}\frac{dp}{dz} \tag{1}$$

$$u_z=\frac{1}{\mu}\frac{dp}{dz}\left(\frac{r^2}{4}+c_1\ln r+c_2\right) \tag{2}$$

In above equation, the velocity is limited at r = 0, therefore, $c_1$=0. The total equations of the first/second orders boundary conditions are:

$$u_z\,|_{r=r_2}=-\frac{2-\sigma}{\sigma}\lambda\frac{\partial u_z}{\partial r}\,|_{r=r_2} \tag{3}$$

$$u_z|_{r=r_2} = -\frac{2-\sigma}{\sigma}\lambda\frac{\partial u_z}{\partial r}|_{r=r_2} + A_2\lambda^2\frac{\partial^2 u_z}{\partial r^2}|_{r=r_2} \quad (4)$$

Assuming $Kn = \frac{\lambda}{2r_2}$ and applying boundary conditions (equations (3-4)) in equation 2, the velocity equations are obtained:

$$u_z = \frac{r_2^2}{4\mu}(-\frac{dp}{dz})[1-(\frac{r}{r_2})^2 + 4\frac{2-\sigma}{\sigma}Kn] \quad (5)$$

$$u_z = \frac{r_2^2}{4\mu}(-\frac{dp}{dz})[1-(\frac{r}{r_2})^2 + 4\frac{2-\sigma}{\sigma}Kn - 8A_2Kn^2] \quad (6)$$

## Parallel Plate/Rectangular microchannel

According to Figures 1(b-c), the total momentum equation for parallel plate/rectangular microchannel is:

$$\frac{\partial^2 u_z}{\partial y^2} = \frac{1}{\mu}\frac{dp}{dz} \quad (7)$$

$$u_z = \frac{1}{\mu}\frac{dp}{dz}(\frac{y^2}{2} + a_2 y + a_2) \quad (8)$$

The total equations of the first/second orders boundary conditions are:

$$u_z|_{y=+h} = -\frac{2-\sigma}{\sigma}\lambda\frac{\partial u_z}{\partial y}|_{y=+h} \quad (9)$$

$$u_z|_{y=+h} = -\frac{2-\sigma}{\sigma}\lambda\frac{\partial u_z}{\partial y}|_{y=+h} + A_2\lambda^2\frac{\partial^2 u_z}{\partial y^2}|_{y=+h} \quad (10)$$

In the center of micro-channel: $\left|\frac{\partial u_z}{\partial y}\right|_{y=0} = 0$, therefore, $a_1$=0. For the parallel plates microchannel, m>>h then $Kn = \frac{\lambda}{4h}$ and applying the boundary conditions (equations (9-10)) in equation 8, the velocity equations are obtained for the first/second-order boundary conditions respectively:

$$u_z = \frac{h^2}{2\mu}(-\frac{dP}{dz})[1-(\frac{y}{h})^2 + 8\frac{2-\sigma}{\sigma}Kn] \quad (11)$$

$$u_z = \frac{h^2}{2\mu}(-\frac{dP}{dz})[1-(\frac{y}{h})^2 + 8\frac{2-\sigma}{\sigma}Kn - 32A_2Kn^2] \quad (12)$$

For the rectangular microchannel $Kn = (\lambda/2h)(1+h/m)$, the velocity equations are:

$$u_z = \frac{h^2}{2\mu}(-\frac{dp}{dz})[1-(\frac{y}{h})^2 + 8\frac{2-\sigma}{\sigma}\frac{Kn}{(1+\frac{h}{m})}] \quad (13)$$

$$u_z = \frac{h^2}{2\mu}(-\frac{dp}{dz})[1-(\frac{y}{h})^2 + 8\frac{2-\sigma}{\sigma}\frac{Kn}{(1+\frac{h}{m})} - 32A_2\frac{Kn^2}{(1+\frac{h}{m})^2}] \quad (14)$$

Van der Waals Equation is one of the important state equations for non-ideal gas: [11,24]

$$P = \rho RT\left(1 + B\rho + C\rho^2 + D\rho^3\right) \quad (15)$$

Where

$$B = \left(b - \frac{a}{RT}\right) \quad (16)$$

$$C = b^2 \quad (17)$$

$$D = b^3 \quad (18)$$

$$a = \frac{27}{64}\frac{R^2T_C^2}{P_C} \quad (19)$$

$$a = \frac{RT_C}{8P_C} = \frac{V_C}{3} \quad (20)$$

By derivation of the sides of equation (15) to z and substituting in equations (5), (6), (11), (12), (13), and (14), the velocity equations in terms of the first and second order boundary conditions for each geometry are shown in Table 1:

**Table 1**
Velocity equations for circular, plate/rectangular micro-channels.

| Geometry type | First-Order Velocity Equation | Second-Order Velocity Equation |
|---|---|---|
| Circular microchannel | $u_z = \frac{-{r_2}^2}{4\mu}\ [RT(1+2B\rho+3C\rho^2+4D\rho^3)]$ $\left[1-(\frac{r}{r_2})^2+4\frac{(2-\sigma)}{\sigma}Kn\right]d\rho/dz$ (21) | $u_Z = \frac{-{r_2}^2}{4\mu}\ [RT(1+2B\rho+3C\rho^2+4D\rho^3)]$ $\left[1-(\frac{r}{r_2})^2+4\frac{(2-\sigma)}{\sigma}Kn-8A_2Kn^2\right]d\rho/dz$ (22) |
| Parallel plate microchannel | $u_Z = \frac{-h^2}{2\mu}\ [RT(1+2B\rho+3C\rho^2+4D\rho^3)]$ $\left[1-(\frac{y}{h})^2+8\frac{(2-\sigma)}{\sigma}Kn\right]d\rho/dz$ (23) | $u_Z = \frac{-h^2}{2\mu}\ [RT(1+2B\rho+3C\rho^2+4D\rho^3)]$ $\left[1-(\frac{y}{h})^2+8\frac{(2-\sigma)}{\sigma}Kn-32A_2Kn^2\right]d\rho/dz$ (24) |
| Rectangular microchannel | $u_Z = \frac{-h^2}{2\mu}\ [RT(1+2B\rho+3C\rho^2+4D\rho^3)]$ $\left[1-(\frac{y}{h})^2+8\frac{(2-\sigma)}{\sigma}\frac{Kn}{(1+\frac{h}{m})}\right]d\rho/dz$ (25) | $u_Z = \frac{-h^2}{2\mu}\ [RT(1+2B\rho+3C\rho^2+4D\rho^3)]$ $\left[1-(\frac{y}{h})^2+8\frac{(2-\sigma)}{\sigma}\frac{Kn}{(1+\frac{h}{m})}-32A_2\frac{Kn^2}{(1+\frac{h}{m})^2}\right]d\rho/dz$ (26) |

## FORMULATION

### Circular microchannel

Definition:

$$u_{z0} = \frac{-{r_2}^2}{4\mu}\ \frac{dP}{dz} = \frac{-{r_2}^2}{4\mu}\ [(1+2B\rho+3C\rho^2+4D\rho^3)]d\rho/dz \quad (27)$$

$$u_z^* = \frac{u_z}{u_{Z0}} \quad (28)$$

$$r^* = \frac{r}{r_2} \quad (29)$$

$u_{z_0}$is velocity in the center of circular microchannel. Substituting equations (21), (22), (27) ,and (29) in equation (28) and substituting the velocity profile on the cross-section, the mean velocity is obtained as follows:

$$\overline{u_z^*} = \frac{1}{2}+4\frac{(2-\sigma)}{\sigma}Kn \quad (30)$$

$$\overline{u_z^*} = \frac{1}{2}+4\frac{(2-\sigma)}{\sigma}Kn-8A_2Kn^2 \quad (31)$$

### Parallel Plates microchannel

Definition:

$$u_{z_0} = \frac{-h^2}{2\mu}\ \frac{dP}{dz} = \frac{-h^2}{2\mu}\ [(1+2B\rho+3C\rho^2+4D\rho^3)]d\rho/dz \quad (32)$$

$$y^* = \frac{y}{h} \quad (33)$$

Substituting equations (32-33), (23-24) in equation 28 and integrating the velocity profile on the cross-section, the mean velocity is obtained as follows:

$$\overline{u_z^*} = \frac{2}{3}+8\frac{(2-\sigma)}{\sigma}Kn \quad (34)$$

$$\overline{u_z^*} = \frac{2}{3}+8\frac{(2-\sigma)}{\sigma}Kn-32A_2Kn^2 \quad (35)$$

### Rectangular Microchannel

For rectangular microchannel, equations (25-26), (34-35) are substituted in equation 28 and by integrating the velocity profile on the cross-section, the mean velocity:

$$\overline{u_Z^*} = \frac{2}{3}+8\frac{(2-\sigma)}{\sigma}\frac{Kn}{(1+\frac{h}{m})} \quad (36)$$

$$\overline{u_Z^*} = \frac{2}{3}+8\frac{(2-\sigma)}{\sigma}\frac{Kn}{(1+\frac{h}{m})}-32A_2\frac{Kn^2}{(1+\frac{h}{m})^2} \quad (37)$$

The general form of the mass flow rate equation:

$$\dot{m} = \rho\overline{u_z}A \ \Rightarrow\ \overline{u_z} = \frac{\dot{m}}{\rho A} \quad (38)$$

Considering the following equation:

$$\overline{u_z} = \overline{u_z^*}\times u_{Z0} \quad (39)$$

Substituting equation 38 in equation 39, mass flow rate equation in terms of the first and second order boundary conditions and by defining the right side variables in Table 2, the equation 40 is obtained. Table 2 shows coefficient values for circular, parallel plate and rectangular microchannels in equation 40.

## SLIP-FLOW MODELS

The Poiseuille number is described as the dimensionless mean wall shear stress and depends on hydraulic diameter. (equation 41). Substituting mean velocity (equation 39) and hydraulic diameter for each geometries in equation 41, Po correlations are obtained for the first/second orders slip velocity boundary conditions.

$$Po = -\frac{D_H^2}{2\mu}\frac{dp}{dz}\frac{1}{\bar{u}_z} \tag{41}$$

## VALIDATION

To validate the analytical results, equation 40 is solved for ideal gas (b = 0). Replacing the right side variables at Table 2 into equation 40 and using the ideal gas state equation $(P = \rho RT)$ , the mass flow rate equation is obtained for the ideal gas flow in microchannel. Tables(4-5) show a comparison of the values of mass flow rate for ideal gas flow in different shapes of microchannels under the first/second orders boundary conditions with a solution of the integral equation in Ref [25]. The results illustrate the accuracy of equation 40.

## RESULTS AND DISCUSSION

In this section, equation 40 has been solved and the results are presented. It is assumed that non ideal gas is $CO_2$ and its properties are R=188.92(J/Kg.0K), μ=1.74×10-5(N.s)/m$^2$, $\rho_i$= 1.517(Kg/m3), $\upsilon_c$= 0.002139(m3/Kg) ,T=350°k.The hydraulic diameter for each geometry is 10 μm.

Tables 6, 7 and 8 show that the $\prod$ values for the first/second orders boundary conditions in terms of the microchannel length in the Knudsen numbers, Kn=$10^{-3}$,Kn=$10^{-2}$ ,and Kn=$10^{-3}$ respectively.According to the tables, with the increase of the length of the microchannel at various Knudsen numbers and as well as the increase of Knudsen number in a specified length, the values of the ratio of density to inlet density decrease and increase, respectively. In other words, the rarefication process occurs faster at low Knudsen numbers. Comparison between tables show that $\prod$ values for parallel plates microchannel in a specified length is more than the other microchannel geometries.This means that the rarefication process in microchannel with circular cross section geometry occurs faster than the others. At various length, $\prod$ values for second order slip model is more than the first order slip model approximately.

The comparison $\prod$ values between ideal and non-ideal gaseous slip flow is indicated in tables 9 and 10. According to results, in L=50mm, $\prod$ values of non-ideal gas are more than ideal gas in different Knudsen numbers and geometries for the first/second orders boundary conditions. In other words, the rarefication process of ideal-gas occurs faster than the non-ideal gas. Also, for ideal gas, $\prod$ valus of parallel plates microchannel is more than others.

**Table 2**
coefficient values for shapes of different microchannel.

| **Geometry type** | **Cross section area** | $\alpha_5\prod^5 + \alpha_4\prod^4 + \alpha_3\prod^3 + \alpha_2\prod^2 = 1/\alpha_1 + \alpha/\alpha_1$ (40) | | |
|---|---|---|---|---|
| Circular microchannel | $A = \pi r_2^2$ | First-Order | $\alpha_1 = \frac{-\pi r_2^4 RT}{4\mu\dot{m}L} \times \left(\frac{1}{2} + 4\frac{(2-\sigma)}{\sigma}Kn\right)$ | $\prod = \rho/\rho_i$<br>$\alpha_2 = \frac{1}{2}\rho_i^2$<br>$\alpha_3 = \frac{2}{3}B\rho_i^3$<br>$\alpha_4 = \frac{3}{4}C\rho_i^4$<br>$\alpha_5 = \frac{4}{5}D\rho_i^5$<br>$\alpha/\alpha_1 = \alpha_2 + \alpha_3 + \alpha_4 + \alpha_5$ |
| | | Second-Order | $\alpha_1 = \frac{-\pi r_2^4 RT}{4\mu\dot{m}L} \times \left(\frac{1}{2} + 4\frac{(2-\sigma)}{\sigma}Kn - 8A_2Kn^2\right)$ | |
| Parallel plates microchannel | $A = 4m.h$ | First-Order | $\alpha_1 = \frac{-4m.h^3.RT}{2\mu\dot{m}L} \times \left(\frac{2}{3} + 8\frac{(2-\sigma)}{\sigma}Kn\right)$ | |
| | | Second-Order | $\alpha_1 = \frac{-4m.h^3 RT}{2\mu\dot{m}L} \times \left(\frac{2}{3} + 8\frac{(2-\sigma)}{\sigma}Kn - 32A_2Kn^2\right)$ | |
| Rectangular microchannel | $A = 4m.h$ | First-Order | $\alpha_1 = \frac{-4m.h^3.RT}{2\mu\dot{m}L} \times \left(\frac{2}{3} + 8\frac{(2-\sigma)}{\sigma}\frac{Kn}{(1+\frac{h}{m})}\right)$ | |
| | | Second-Order | $\alpha_1 = \frac{-4mh^3 RT}{2\mu\dot{m}L} \times \left(\frac{2}{3} + 8\frac{(2-\sigma)}{\sigma}\frac{Kn}{(1+\frac{h}{m})} - 32A_2\frac{Kn^2}{(1+\frac{h}{m})^2}\right)$ | |

**Table 3**
Po correlation for first/second orders slip velocity boundary conditions.

| Geometry type | First-Order Poiseuille number | Second-Order Poiseuille number |
|---|---|---|
| Circular microchannel | $Po = \frac{8}{\left[\frac{1}{2} + 4\frac{(2-\sigma)}{\sigma}Kn\right]}$ (42) | $Po = \frac{8}{\left[\frac{1}{2} + 4\frac{(2-\sigma)}{\sigma}Kn - 8A_2Kn^2\right]}$ (43) |
| Parallel plates microchannel | $Po = \frac{24}{\left[1 + 12\frac{(2-\sigma)}{\sigma}Kn\right]}$ (44) | $Po = \frac{24}{\left[1 + 12\frac{(2-\sigma)}{\sigma}Kn - 48A_2Kn^2\right]}$ (45) |
| Rectangular microchannel | $Po = \frac{24}{(1+\frac{h}{m})^2\left[1 + 12\frac{(2-\sigma)}{\sigma}\frac{Kn}{(1+\frac{h}{m})}\right]}$ (46) | $Po = \frac{24}{(1+\frac{h}{m})^2\left[1 + 12\frac{(2-\sigma)}{\sigma}\frac{Kn}{(1+\frac{h}{m})} - 48A_2\frac{Kn^2}{(1+\frac{h}{m})^2}\right]}$ (47) |

**Table 4**
mass flow rate for first order boundary conditions

| Geometry type | Kn=0.001 | | Kn=0.01 | | Kn=0.1 | |
|---|---|---|---|---|---|---|
| | Present study | Ref.(25) | Present study | Ref.(25) | Present study | Ref.(25) |
| Circular microchannel | 1.28954E-25 | 1.28845E-25 | 1.38165E-25 | 1.38912E-25 | 2.30275E-25 | 2.30454E-25 |
| Parallel plates microchannel | 3.43594E-26 | 3.43678E-26 | 3.80261E-26 | 3.80456E-26 | 7.46943E-26 | 7.46565E-26 |
| Rectangular microchannel | 3.42236E-26 | 3.42899E-26 | 3.66681E-26 | 3.66780E-26 | 6.11135E-26 | 6.11456E-26 |

**Table 5**
mass flow rate for second order boundary conditions.

| Geometry type | Kn=0.001 | | Kn=0.01 | | Kn=0.1 | |
|---|---|---|---|---|---|---|
| | Present study | Ref.(25) | Present study | Ref.(25) | Present study | Ref.(25) |
| Circular microchannel | 1.28956E-25 | 1.28364E-25 | 1.38395E-25 | 1.38121E-25 | 2.53303E-25 | 2.53468E-25 |
| Parallel plates microchannel | 3.43612E-26 | 3.43001E-26 | 3.82095E-26 | 3.82778E-26 | 9.30283E-26 | 9.30570E-26 |
| Rectangular microchannel | 3.42243E-26 | 3.42678E-26 | 3.67495E-26 | 3.67065E-26 | 6.92619E-26 | 6.92238E-26 |

**Table 6**
Values of Π for first /second orders boundary conditions in terms of circular microchannel length.

| L(mm) | First-Order Slip Model | | | Second-Order Slip Model | | |
|---|---|---|---|---|---|---|
| | $Kn=10^{-3}$ | $Kn=10^{-2}$ | $Kn=10^{-1}$ | $Kn=10^{-3}$ | $Kn=10^{-2}$ | $Kn=10^{-1}$ |
| 0 | 0.999998477 | 0.999998477 | 0.999998477 | 0.999998477 | 0.999998477 | 0.999998477 |
| 30 | 0.928023277 | 0.932846271 | 0.960391161 | 0.927998628 | 0.933085677 | 0.964015134 |
| 50 | 0.876765486 | 0.885254489 | 0.933053294 | 0.876722004 | 0.885674892 | 0.939261191 |
| 100 | 0.733115434 | 0.753240446 | 0.860921443 | 0.733011435 | 0.754228116 | 0.874317434 |

**Table 7**
Values of Π for first/second orders boundary conditions in terms of parallel plates microchannel length.

| L(mm) | First-Order Slip Model | | | Second-Order Slip Model | | |
|---|---|---|---|---|---|---|
| | $Kn=10^{-3}$ | $Kn=10^{-2}$ | $Kn=10^{-1}$ | $Kn=10^{-3}$ | $Kn=10^{-2}$ | $Kn=10^{-1}$ |
| 0 | 0.999998477 | 0.999998477 | 0.999998477 | 0.999998477 | 0.999998477 | 0.999998477 |
| 30 | 0.983582209 | 0.985177116 | 0.992480698 | 0.983583093 | 0.985248765 | 0.9939668 |
| 50 | 0.972484187 | 0.97517115 | 0.987437068 | 0.972485676 | 0.975291787 | 0.989925278 |
| 100 | 0.944168951 | 0.949695415 | 0.974713894 | 0.944172018 | 0.94994314 | 0.979748583 |

**Table 8**
Values of Π for first/second orders boundary conditions in terms of rectangular microchannel length.

| L(mm) | First-Order Slip Model | | | Second-Order Slip Model | | |
|---|---|---|---|---|---|---|
| | $Kn=10^{-3}$ | $Kn=10^{-2}$ | $Kn=10^{-1}$ | $Kn=10^{-3}$ | $Kn=10^{-2}$ | $Kn=10^{-1}$ |
| 0 | 0.999998477 | 0.999998477 | 0.999998477 | 0.999998477 | 0.999998477 | 0.999998477 |
| 30 | 0.967171178 | 0.969394228 | 0.981750346 | 0.967170384 | 0.96932499 | 0.978912768 |
| 50 | 0.94465317 | 0.948443276 | 0.969394228 | 0.944651814 | 0.948325328 | 0.964599758 |
| 100 | 0.885859029 | 0.893921567 | 0.937792403 | 0.885856136 | 0.893671272 | 0.927852384 |

**Table9**
Comparison of ∏ values between ideal and non ideal gaseous flow for first boundary conditions in L=5mm.

| Geometry type | Ideal Gas | | | Non-Ideal Gas | | |
|---|---|---|---|---|---|---|
| | $Kn=10^{-3}$ | $Kn=10^{-2}$ | $Kn=10^{-1}$ | $Kn=10^{-3}$ | $Kn=10^{-2}$ | $Kn=10^{-1}$ |
| Circular | 0.8765537157 | 0.8853027846 | 0.9327822874 | 0.876765486 | 0.885254489 | 0.933053294 |
| Parallel plate | 0.9722801040 | 0.9749659394 | 0.9872266730 | 0.972484187 | 0.97517115 | 0.987437068 |
| Rectangular | 0.9444605796 | 0.9482491399 | 0.9691914373 | 0.94465317 | 0.948443276 | 0.969394228 |

**Table10**
Comparison of ∏ values of ideal and non ideal gaseous flow for second boundary conditions in L=5mm.

| Geometry type | Ideal Gas | | | Non-Ideal Gas | | |
|---|---|---|---|---|---|---|
| | $Kn=10^{-3}$ | $Kn=10^{-2}$ | $Kn=10^{-1}$ | $Kn=10^{-3}$ | $Kn=10^{-2}$ | $Kn=10^{-1}$ |
| Circular | 0.8765560709 | 0.8855055592 | 0.9390707889 | 0.876722004 | 0.885674892 | 0.939261191 |
| Parallel plate | 0.9722815923 | 0.9750865259 | 0.9897138232 | 0.972485676 | 0.975291787 | 0.989925278 |
| Rectangular | 0.9444592237 | 0.9481312399 | 0.9643989645 | 0.944651814 | 0.948325328 | 0.964599758 |

Figures (2-4) show the fully developed velocity profiles in different Knudsen numbers under the first/second orders slip boundary conditions at L=50 mm. According to these Figures with the increase of the knudsen number, velocity values in the center and boundaries increased, so that the maximum of velocity values are in center of microchannel and the its lowest are at the boundary for each geometry. In high knudsen numbers, (Kn=0.05 and more) the velocity values for the second order boundary conditions are more than the first order boundary condition.

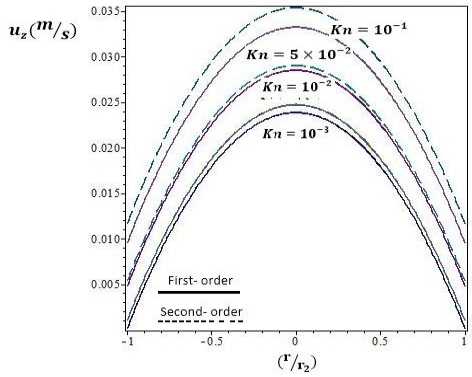



**Fig. 2.** The developed velocity profile of circular microchannel in different Knudsen number

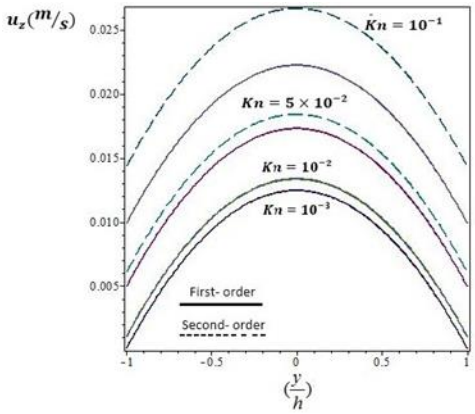



**Fig. 3.** The developed velocity profile of parallel plate microchannel in different Knudsen numbers

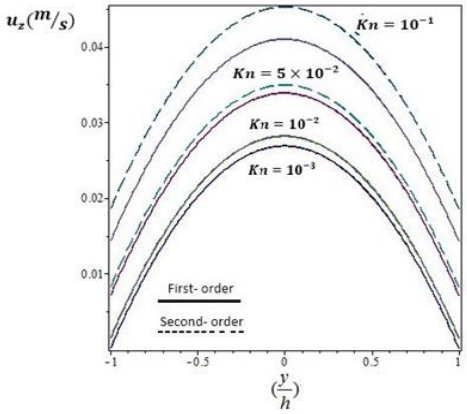



**Fig. 4.** The developed velocity profile of rectangular microchannel in different Knudsen numbers

In Figure 5, the fully developed velocity profiles have been compared in circular, parallel plate and rectangular microchannels under the second order slip boundary conditions in Kn=0.05. Results show that the rectangular microchannel has maximum velocity values in center and wall than others.

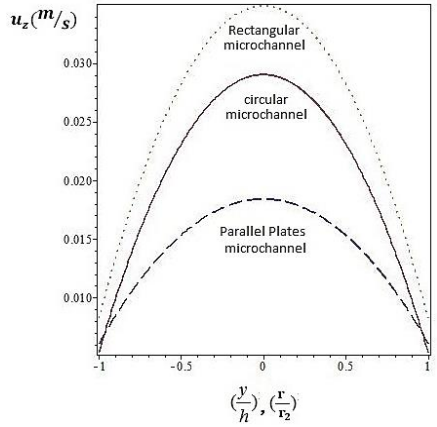



**Fig. 5.** The developed velocity profile for three geometries underthe second orders slip boundary conditions in Kn=0.05

In Figures 6, 7 and 8, the mass flow rate in terms of the density to inlet density ratios have been shown for the first/second order boundary conditions, at L=50 mm.

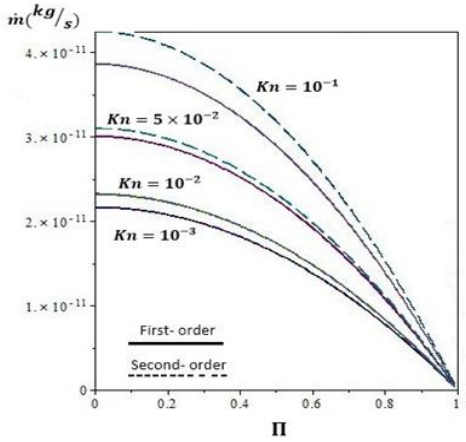



**Fig. 6.** The mass flow rate in terms of density ratio for circular microchannel

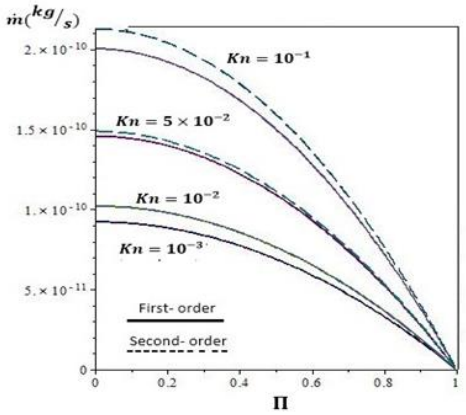



**Fig. 7.** The mass flow rate in terms of density ratio for parallel plate microchannel

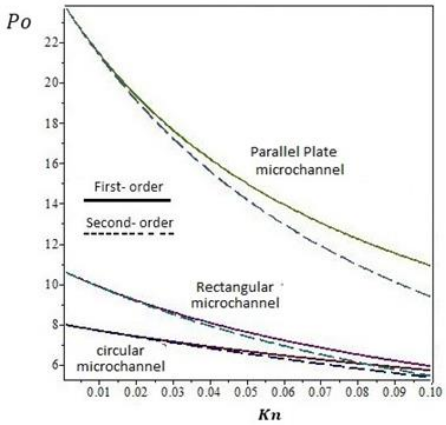



**Fig. 8.** Poiseuille number in terms of Knudsen number for three geometries.

According to these Figures, with increasing density ratio, the mass flow rate decreases, exponentially. With increasing Knudsen number, the mass flow rates for first-order boundary conditions are lower than the second-order boundary conditions.

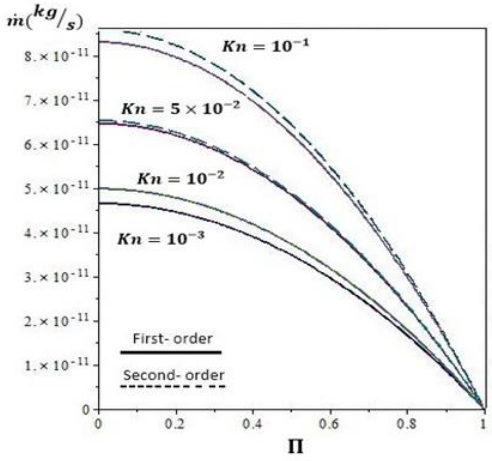



**Fig. 9.** The mass flow rate in terms of density ratio for rectangular microchannel

Figure 9 represents comparison with the mass flow rate in terms of density ratio for circular, parallel plates and rectangular microchannels under the second order slip boundary conditions at Kn=0.05. According to Results, the rectangular microchannel has maximum mass flow rate in comparison to the others.

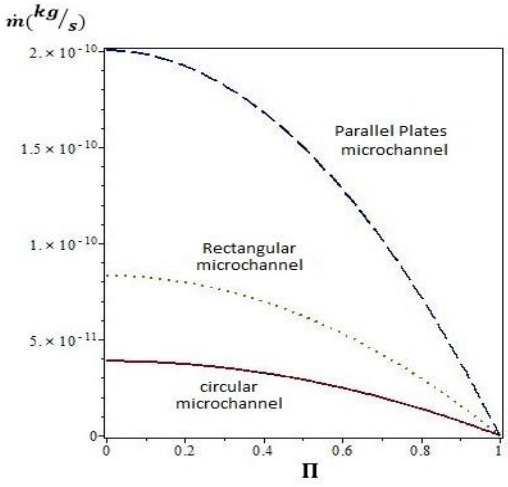



**Fig. 10.** The mass flow rate in terms of density ratio for three geometries under the second orders slip boundary conditions at Kn=0.05

The Poiseuille number in terms of Knudsen number under first/second-order boundary conditions for different microchannels are shown in Figure 10. The results show that Poiseuille number decreases with the increasing Knudsen number. For various Knudsen numbers, changes of

Poiseuille numbers in terms of the Knudsen numbers for the parallel plates microchannel are more than the others.

## CONCLUSION

In this paper, a fully developed non-ideal gas flow through circular, parallel plate and rectangular microchannels is analytically analyzed. This study is carried out under the first and second orders slip velocity boundary conditions by using the Navier- Stokes equations.

It is presented the models for predicting the local and mean velocity, normalized Poiseuille number, mass flow rate, and the ratio of density. According to results:

1. The rarefication process is a function of the Knudsen number and the cross-section geometry and is a weak function of the type of gases. Poiseuille number is independent of fluid material properties, velocity, and temperature and is a function of the cross-section geometry.
2. The values of $\prod$ are almost the same for both the first and second order boundary conditions. Therefore, the use of second order boundary conditions has no effect on the $\prod$ values at circular, parallel plate and rectangular microchannels.
3. For the microchannel with circular cross-section geometry, the rarefication process occurs faster than the others for both the first / second order boundary condition and ideal / non-ideal gas.
4. For the first/second orders boundary conditions, the values of the velocities and the mass flow rate are same in Knudsen numbers less than 0.01.

## REFERENCES


[1] Arkilic E, Schmidt M, Member, IEEE, Breuer, K. Gaseous Slip Flow in Long Microchannels.1997;167-178.

[2] Ebert W, Sparrow EM. Slip flow in rectangular and annular ducts. Journal of Basic Engineering. 1965;87(4):1018-24.

[3] Morini GL, Spiga M, Tartarini P. The rarefaction effect on the friction factor of gas flow in microchannels. Superlattices and microstructures. 2004;35(3-6):587-99.

[4] Vimmr J, Klášterka H, Hajžman M. Analytical solution of gaseous slip flow between two parallel plates described by the Oseen equation. Mathematics and Computers in Simulation. 2012;82(10):1832-40.

[5] Duan Z, Muzychka Y. Slip flow in elliptic microchannels. International Journal of Thermal Sciences. 2007;46(11):1104-11.

[6] Duan Z, Muzychka Y. Slip flow in non-circular microchannels. Microfluidics and Nanofluidics. 2007;3(4):473-84.

[7] Das SK, Tahmouresi F. Analytical solution of fully developed gaseous slip flow in elliptic microchannel. Int J Adv Appl Math and Mech 3i. 2016:1-15.

[8] Duan Z, Yovanovich M, editors. Models for gaseous slip flow in circular and noncircular microchannels. ASME 2010 8th International Conference on Nanochannels, Microchannels, and Minichannels collocated with 3rd Joint US-European Fluids Engineering Summer Meeting; 2010: American Society of Mechanical Engineers.

[9] Tahmouresi F, Das SK .Analytical modeling of gaseous slip flow in parabolic microchannels. Journal of Fluids Engineering. 2014;136(7):071201.

[10] Wang M, Li Z. An Enskog based Monte Carlo method for high Knudsen number non-ideal gas flows. Computers & fluids. 2007;36(8):1291-7.

[11] Shi Y, Zhao T, Guo Z. Lattice Boltzmann simulation of dense gas flows in microchannels. Physical Review E. 2007;76(1):016707.

[12] He X, Shan X, Doolen GD. Discrete Boltzmann equation model for nonideal gases. Physical Review E. 1998;57(1):R13.

[13] Ihle T, Kroll D. Thermal lattice-Boltzmann method for non-ideal gases with potential energy. Computer physics communications. 2000;129(1-3):1-12.

[14] Hosseinalipour S, Jabbari E, Madadelahi M, Fardad A. Gas Mixing Simulation in a T-Shape Micro Channel Using The DSMC Method. Transp Phenom Nano Micro Scales. 2014;2(2):132-9.

[15] Hong C, Asako Y, Matsushita S, Ueno I, editors. Flow and Heat Transfer Characteristics of Turbulent Gas Flow in Microtube with Constant Heat Flux. Journal of Physics: Conference Series; 2012: IOP Publishing.

[16] Hong C, Asako Y, Ueno I, Motosuke M. Total temperature measurement of laminar gas flow at microtube outlet: cooled from the wall. Heat Transfer Engineering. 2014;35(2):142-9.

[17] Kawashima D, Asako Y. Measurement of quasi-local friction factor of gas flow in a micro-tube. Proceedings of the Institution of Mechanical Engineers, Part C: Journal of Mechanical Engineering Science. 2016;230(5):782-92.

[18] Rovenskaya O. Computational study of 3D rarefied gas flow in microchannel with 90 bend. European Journal of Mechanics-B/Fluids. 2016;59:7-17.

[19] Li H, Hrnjak P. Effect of channel geometry on flow reversal in microchannel evaporators. International Journal of Heat and Mass Transfer. 2017;115:1-10.

[20] Li H, Hrnjak P. Effect of refrigerant thermophysical properties on flow reversal in microchannel evaporators. International Journal of Heat and Mass Transfer. 2018;117:1135-46.

[21] Monsivais I, Lizardi J, Méndez F. Conjugate thermal creep flow in a thin microchannel. International Journal of Thermal Sciences. 2018;124:227-39.

[22] Holagh SG, Talati F, Shamsaiee M. Analytical solution of steady state heat conduction equations in irregular Domains with various BCs by use of Schwarz-Christoffel conformal mapping. Thermal Science and Engineering Progress. 2019;11:8-18.

[23] Yang DY, editor Analytical solution of mixed electroosmotic and pressure-driven flow in

rectangular microchannels. Key Engineering Materials; 2011: Trans Tech Publ.

[24] Wang M, Li Z. Nonideal gas flow and heat transfer in micro-and nanochannels using the direct simulation Monte Carlo method. Physical Review E. 2003;68(4):046704.

[25] Kandlikar S,Garimella S,Li D,Colin S,King M.Heat Transfer and Fluid Flow in Minichannels and Microchannels.elsevier.2005.